Design and Implementation of Scalable 6.5 GHz Reconfigurable Intelligent Surface for Wi-Fi 6E

Nuno Paulino*, Francisco M. Ribeiro*, Luís Outeiro*, Pedro A. Lopes† Sofia Inácio* Luís M Pessoa*
*INESC TEC, Faculty of Engineering, University of Porto, Porto, Portugal, nuno.m.paulino@inesctec.pt
†INESC TEC, Porto, Portugal

***Abstract*—Wi-Fi 6E will enable dense communications with low latency and high throughput, meeting the demands of ever growing network traffic and supporting emergent services such as ultra HD or multi-video streaming, and augmented or virtual reality. However, the 6 GHz band suffers from higher path loss and signal attenuation, and poor performance in NLoS conditions. Reconfigurable Intelligent Surfaces (RISs) can address these challenges by providing low-cost directional communications with increased spectral and energy efficiency. However, RIS designs for the WiFi-6E range are under-explored in literature. We present the implementation of an 8x8 RIS tuned for 6.5 GHz designed for scalability. We characterize the response of the unit cell, and evaluate the RIS in an anechoic chamber, measuring the far field radiation patterns for several digital beamsteering configurations in a horizontal plane, demonstrating effective signal steering.**

***Index Terms*—reconfigurable intelligent surface, reflect-array, WiFi-6E, antennas, beamsteering**

I. Introduction

The Wi-Fi 6E standard was defined to extend Wi-Fi to the 5.925 GHz to 7.125 GHz range [1]. This bandwidth provides up to 7 160 MHz channels, versus the 2 channels of this bandwidth available in both Wi-Fi 5 and Wi-Fi 6. Alternatively, up to 59 20 MHz channels are possible. This will enable support for denser networks with less congestion relative to the crowded Wi-Fi 5 spectrum, and can deliver a throughput of up to 9.6 Gbps. However, the 6 GHz band suffers from short range and poor operation in NLoS conditions [2]. Increased power consumption is required to compensate for this shorter range, and indoor scenarios with walls and obstructions may require additional nodes to act as repeaters, increasing costs.

RISs are composed by a matrix of antenna elements, also called unit cells. These devices contain no active RF chains, and instead rely simpler electronics to change the reflection coefficient of the unit cells. The control of all unit cells determines the reflection phase of impinging signal, and thus control of the wireless environment [3]. This can be used to implement beamforming, i.e., to direct a reflected signal only towards an intended direction. The advantages are increased spectral efficiency and power consumption, by reducing radiation towards unintended directions, and support for NLOS communications, since links can be redirected around obstacles. These advantages position RIS' as a potential low-cost solution to the challenges of of Wi-Fi 6E. Furthermore, RIS' have also been used to support other Wi-Fi based applications like localization [4] and imaging [5]. However, RIS designs for Wi-Fi 6E are under-explored in literature.

In this paper, we present the design and fabrication of a unit cell for a RIS, tuned for 6.5 GHz and with a 1-bit phase control. We measure the achieved magnitude and phase response of the unit cell in a waveguide environment, and evaluate a 8x8 RIS tile in anechoic chamber, characterizing the radiation pattern for different frequencies and steering angles.

This work was carried out in the framework of the SUPERIOT project, which received funding from the Smart Networks and Services Joint Undertaking (SNS JU) under the European Union's Horizon Europe research and innovation programme under Grant Agreement No 101096021, including funding under the UK government's Horizon Europe funding guarantee, UKRI Grant Reference Number 10053751.

II. Related Work

In [6] a RIS design for 3.5 GHz is evaluated in a real-world environment. The design is fabricated on 1.52 mm thick F4BT450 substrate, and contains 2430 unit cells in a near square layout. A varactor is employed per unit cell to achieve a phase control range of close to 360°. The experimental setup consisted of an RX in non-line-of-sight from the TX, and used an SDR implementation to stream data using QPSK modulation. The RIS and RX were placed at three different relative orientations to demonstrate the RIS steering capabilities.

A RIS tuned for 5.8 GHz with 16x10 elements is presented in [7]. Using one PIN diode per elementa phase difference of 171° between states is achieved. The design uses a single layer Rogers RT 6002 substrate, and the diodes are controlled by shift-registers and micro-controller on an external PCB. The RIS is evaluated outdoors, with a feed horn placed 5 m away on the same horizontal plane as the RIS. An RX horn placed 10 m away is moved in a quarter circle range, verifying that the RIS improves the SNR at the RX by up to 15 dB.

In [8] the authors present an open-source design for a RIS and unit cell tuned for 5.5 GHz, fabricated on FR4 substrate with three layers. Each unit cell is controlled by a low power RF switch, which sets the unit cell to either a short or open state. An ideal difference of 180° is achieved at the central frequency. The RIS contains 256 elements in a 16x16 disposition, and is controlled by an additional board assembled to its bottom layer which interfaces via USB or Bluetooth.

In [9] focus is on datasets of sub-6 GHz RIS characterization, highlighting that the lack of available datasets hinders research on codebook generation or optimization. They also make available two of their own datasets collected with a

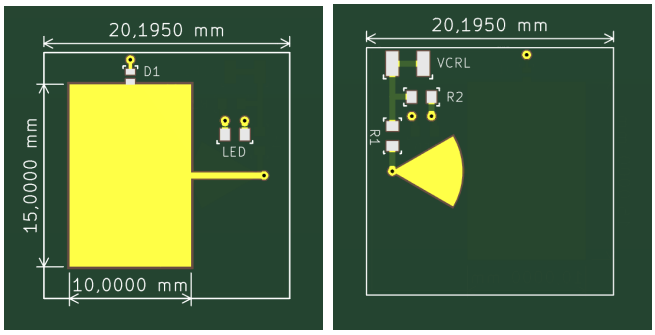

(a) top layer (b) bottom layer

Fig. 1. 6.5 GHz Unit cell design with PIN diode control

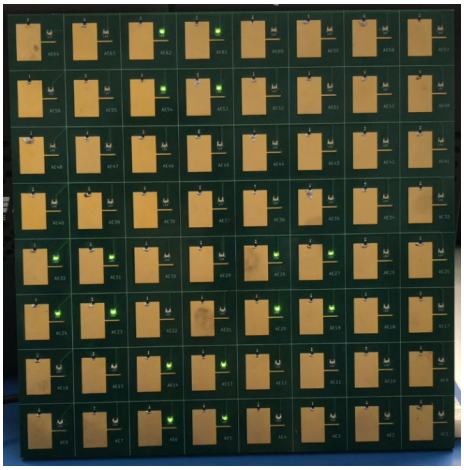

Fig. 2. 64 element RIS tuned for 6.5 GHz, with 1-bit phase control (18.46 cm by 18.46 cm). The status LEDs show some unit cells at the *ON* state.

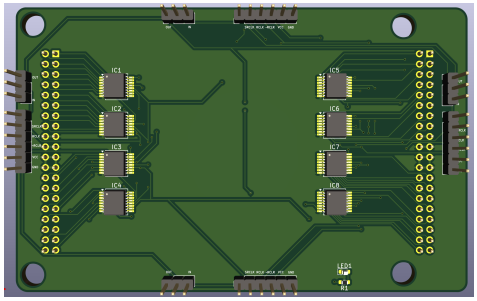

Fig. 3. Top layer of control board hosting shift registers to hold the configuration pattern. Bottom layer contains two 40 male pin-header connectors to interface with the tile.

10x10 5.3 GHz RIS on an FR4 substrate with 0.5 mm thickness. The unit cells rely on SP8T RF switch which enables configuring the phase response to eight different values. Using a setup similar to ours, with the RIS and feed horn mounted on a turntable, the steering performance is characterized for a range of $\pm 90^\circ$ and for sub-arrays of elements of several sizes.

III. Unit Cell and RIS Tile Implementation

A. 6.5Ghz PIN Diode Based Cell Design

The unit cells were designed to be tuned to for a center frequency of 6.5 GHz, corresponding to the central frequency of the WiFi-6E band. Its' top and bottom layer designs are shown in Figure 1. The top layer contains a rectangular patch of 10 mm by 15 mm. The total enclosing perimeter of the design is a square with a side of 23 mm. Placing two cells side by side provides a separation of half a wavelength.

Also shown are the contacts for the *D1* PIN diode used to control the phase response. The control voltage for the PIN diode is applied on the bottom layer (Figure 1b), at *VCRL*. A radial stub is used to decouple the RF path from the DC path.

The PIN diode is an SMP1331-079LF, and the control voltage applied at the *ON* state is of 0.8 V. Given the 220 Ω value for *R1* and the value of 3.3 V applied at *VCRL*, a unit cell in an *ON* state draws 15 mA. Thus, if all PIN diodes are conducting, the RIS consumes 3.16 W, but the majority of control patterns only activates approximately half the unit cells. Resistor *R2* regulates the current for the status LED, which exists to allow for easy interpretation and validation of the applied control pattern throughout the RIS. The LEDs can be disabled globally, but each draws 1 mA if active.

The PCB has a composite substrate, where the top layer is a 4 mm F4B substrate, and the bottom layer is a 0.5 mm FR4 substrate. The cost of a tile totaled approximately 85€ for fabrication, and approximately 60€ for components. The PIN diodes alone are around 50 % of this cost.

B. 8x8 RIS Tile with 6.5 GHz Unit Cell

The fabricated RIS tile is shown in Figure 2. It is composed of 64 units cells designed as shown in Figure 1, resulting in a square design with a side of 18.46 cm. In Figure 2 some of the LEDs, one per unit cell, are active, indicating that the respective unit cell is at its *ON* state, which should ideally produce a 180° of phase shift for the signal reflection. A total of 64 signals are needed to control the entire tile.

The tile allows for easy scalability without compromising ideal beamforming conditions. It was purposefully designed such that when physically placing two tiles side by side, with direct contact between the edges of the PCBs, the spacing between elements at the periphery of both tiles equals then spacing within a single tile. A multi-tile RIS can be assembled by resorting to a mounting structure which secures each tile via its bottom layer, as opposed to any frame based mounting which would physically displace the relative tile positions. We achieve this by assembling two SMD 40-pin female pin header connectors on the bottom layer of the tile. These connectors provide the physical mounting support, specifically by interfacing with a smaller control board, shown in Figure 3.

The control board is 11 cm by 7 cm, and hosts eight shift-registers. Namely, eight 74HC595PW ICs, which are 8-bit serial-in parallel-out shift registers. We have connected these in a daisy chain, and to set these shift registers, the control board contains an SPI interface to an ESP32-S3-DevKitC-1. The ESP32 sends 64 bits to the shift-registers, and issues the a *latch* signal which changes all unit cell configurations simultaneously. This synchronization prevents undesired intermediate

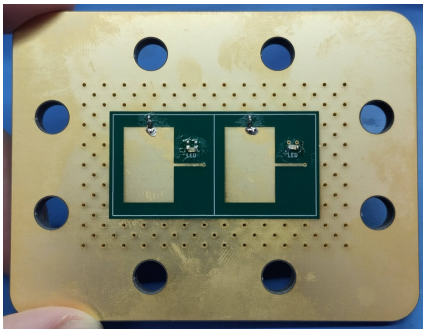

Fig. 4. PCB with two unit cells for validation of frequency and magnitude response in a WR159 waveguide

states which would occur if the values were sent directly to the unit cells as their were being shifted into the tile.

We opt to implement this control board separately from the RIS, instead of assembling the shift-registers on its bottom layer, to mitigate any effects on beamforming performance and to simplify the RIS by homogenizing it, which also simplifies scalability. This separation also allows using the same control board for other RIS designs, e.g., for different unit cell designs. The total cost of the control board is approximately 40€.

Finally, besides allowing for the rear mounting which facilitates the physical scaling of the number of tiles, the four interfaces at the control board's periphery can be interconnected to control additional unit cells. For example, a single ESP32 can command the resulting 256 elements of 4 tiles as a single larger RIS, or four parallel daisy chains can allow for a more explicit tile-level control.

IV. Experimental Evaluation

To evaluate our RIS we first compare the response of the unit cell versus simulations. Based on this analysis, we measure the RIS steering capability in an anechoic chamber.

A. Evaluation of Unit Cell in Waveguide

Figure 4 shows the fabricated PCB for use with a WR159 waveguide, with two unit cells spaced identically to the RIS. To measure the response, we applied the same control to both unit cells via an external voltage source. Figure 5 shows the resulting S11 measurements and respective simulations, for the *ON* and *OFF* states. The simulations considered a Floquet port setup and periodic boundary condition in the 3D electromagnetic simulation software CST, and range from 5.8 GHz to 7.2 GHz, given the intended center frequency of 6.5 GHz. The measurements cover a lower range between 5 GHz to 7 GHz, given the response we observed.

Figure 5a shows the magnitude response. At 6.5 GHz the response for both states is approximately equal, which is a desired behaviour since the reflected power should not depend on the applied control, to avoid any distortions to the desired beamforming. However, the phase difference between states is only 35°, whereas the simulated response was 180°.

Instead, the greatest phase difference of 178° is observed for 5.93 GHz. However, at this frequency the *ON* state experiences

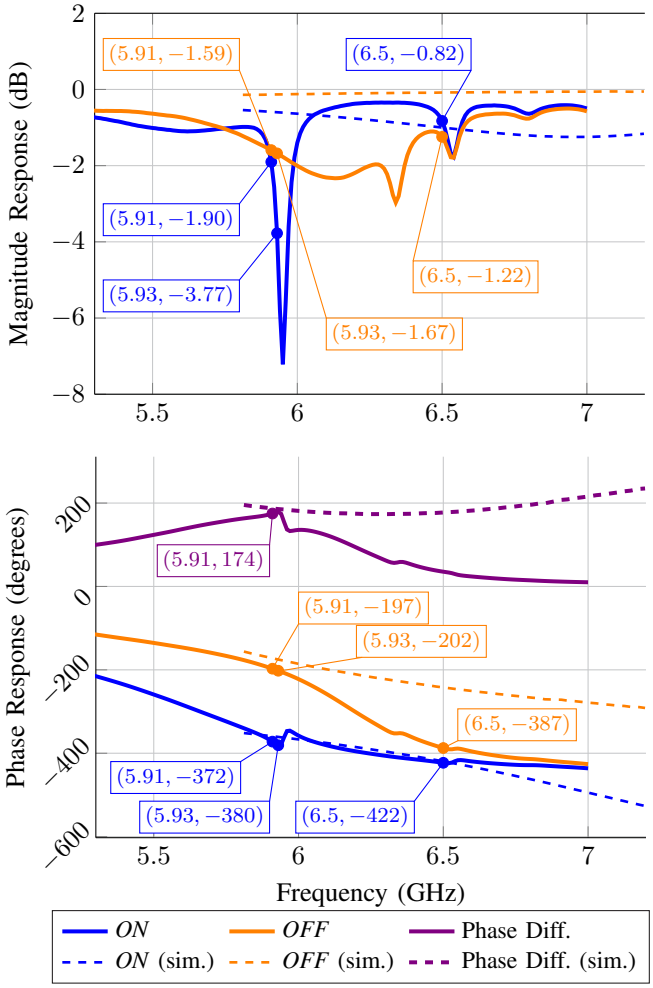

Fig. 5. Magnitude and phase response of unit cell measured in VNA, for both *ON* and *OFF* states. A phase difference closest to 180° is achieved for 5.93 GHz, but a better magnitude response is present at 5.91 GHz.

a −3.77 dB attenuation. Since the magnitude response of the *OFF* state at this frequency is −1.67 dB, the disparity in magnitude response between states could affect beamforming performance. A trade-off between a balanced magnitude response and phase difference occurs for 5.91 GHz, where a 174° phase difference is attained for a more approximate magnitude response between states, and where the response for either state is not lesser than −3 dB.

This deviation may be due to the LED which was not simulated, or to the tolerances of the PIN diode, whose datasheet reports a typical 0.18 pF capacitance up to a maximum of 0.35 pF. However, we note that the magnitude response was extremely sensitive to the alignment between the PCB and the waveguide, with the phase response less so. Additionally, it is known that the waveguide environment imposes an oblique wave incidence condition (of approximately 38° in this case), unlike the normal incidence obtained in free space conditions. Therefore it is difficult to determine precisely the true response that is obtained in free space. In the absence of a better reference, for the following tests of the RIS, we consider

5.91 GHz as the central frequency for computing beamforming control patterns.

B. RIS Characterization in Anechoic Chamber

1) Experimental Setup: Figure 6 shows our setup in an anechoic chamber. We employed two LB-20180-SF horn antennas as the receiver (RX) and feed antenna (TX), and a portable Keysight Fieldfox N9914A VNA to measure the S21 parameters. A single laptop controls the rotor position, RIS configuration, and VNA data gathering.

We consider that the center of the coordinate system is at the center of the RIS, that the XY plane is the broadside of the RIS, and that the direction of the X axis is downwards. The RIS is mounted on a rotating platform, and its X axis is aligned with the rotational axis of this platform.

The feed horn was placed below the RIS, displaced by $25.5\,\mathrm{cm}$ on its X axis, and $36.5\,\mathrm{cm}$ on its Z axis, resulting in a distance of $40\,\mathrm{cm}$ to the feed point phase center. This distance is a compromise between the ideal distance of $20\,\mathrm{cm}$, which would provide an edge tapper of $-9\,\mathrm{dB}$, and a setup that would reduce the occlusion of the RIS by the feed horn. The RX antenna was placed at $170\,\mathrm{cm}$ from the RIS, approximating far field conditions for the measured frequencies.

The RIS control board is attached behind the PCB, containing also the ESP32 micro-controller powered by a power-bank, which receives the pattern to apply to the RIS from a laptop via WiFi (on a $2.4\,\mathrm{GHz}$ link). This laptop computes the configuration based on the desired steering, according to the following equations.

$$R = \sqrt{(x_c - x_{ij})^2 + (y_c - y_{ij})^2 + z_c^2} \tag{1}$$

$$\phi_{ij} = k\left(R - \sin(\theta)x_{ij}\cos(\phi) + y_{ij}\sin(\phi)\right) \tag{2}$$

The coordinates of the feed antenna are given by (x_c, y_c, z_c), which for our case are $(d\sin(35°), 0, d\cos(35°))$, given the distance $d = 400\,\mathrm{mm}$ and $35°$angle of the feed horn towards the RIS. The coordinates of the center of each unit cell, *i, j*, are given by $(x_{ij}, y_{ij}) = (iC_d - \frac{H}{2}, jC_d - \frac{W}{2})$, where C_d is the dimension of the unit cell, $23\,\mathrm{mm}$, and H and W are the height and width of the RIS, both $18.4\,\mathrm{cm}$.

The beam direction is given by θ and ϕ, R is thus the euclidean distance between each unit cell and the feed horn, $k = \frac{2\pi}{\lambda}$ is the wave vector. For these calculations, we considered the wavelength for $5.91\,\mathrm{GHz}$. Finally, given the two control levels available through the PIN diodes, we quantize the resulting ideal phase responses, ϕ_{ij}, to either zero (for $0° < \phi_{ij} < 180°$) or one (for $180° \leq \phi_{ij} \leq 360°$).

With this setup, and considering a frequency range from $5.3\,\mathrm{GHz}$ to $6.5\,\mathrm{GHz}$ (the limit of the VNA) and an angle range of $\pm 60°$ for the rotor position, we performed three measurements of the S21 parameters presented below.

2) Experimental Evaluation: We first retrieved the radiation pattern for RIS configuration of $\theta = 0°$, with a rotor orientation of $0°$ (i.e., forward facing). Our VNA resolution produced measurements for 200 frequencies, and Figure 7 shows the resulting radiation patterns, normalized to $0\,\mathrm{dB}$.

Plotted in light gray are the responses for a subset of all frequencies covering the measured range (specifically, from $5\,\mathrm{GHz}$ to $7\,\mathrm{GHz}$ with a step of $5.9\,\mathrm{MHz}$). We highlighted the previously chosen frequency of $5.91\,\mathrm{GHz}$, and four additional responses in a bandwidth of $\pm 59\,\mathrm{MHz}$. Despite the expected best phase response at this frequency, there is no noticeable steering towards the desired direction of $0°$. Instead, the shown $\pm 50\,\mathrm{MHz}$ bandwidth centered on $6.16\,\mathrm{GHz}$ shows the most response to this steering configuration.

We can attribute this to our measurement of the location of the feed point relative to the RIS center, which is difficult to determine precisely in real world measurements. The calculation of the phase patterns, shown in Equations (1) and (2), depends on these coordinates as well as the presumed central frequency. So, a likely deviation to the true value of (x_c, y_c, z_c) resulted in phase profiles more effective for $6.16\,\mathrm{GHz}$ despite the value of $5.91\,\mathrm{GHz}$ considered for the calculations.

We then measured the radiation patterns for additional RIS configurations, namely $\pm 20°$ and $\pm 40°$. Given the previous conclusion, Figure 8 shows these profiles only for $6.16\,\mathrm{GHz}$ where a good steering response is confirmed. The RIS displays a symmetric behaviour, without angle skew in regards to the steering direction, and with similar magnitude responses for opposing steering angles (e.g. $\pm 20°$.

Despite the good steering response for this frequency, it may not be the best performance achievable by the design. According to the unit cell response for $6.16\,\mathrm{GHz}$ seen in Figure 1, the phase difference between states is of approximately $110°$ and there is a difference of $1.88\,\mathrm{dB}$ between states. That is, although the computed phase profiles generated a good steering response at this frequency, more accurate measurements of the feed point or adjustments to its position could result in a better response for $5.91\,\mathrm{GHz}$, exploiting a greater phase difference between states and therefore resulting in a more focused and power efficient beam.

Finally, we also plot the radiation pattern measured with the RIS disabled, i.e., acting as a purely specular reflector. This shows that there is little passive component received at the RX, for this frequency, and that the previous profiles are a the result of the beamsteering.

V. Conclusion

In this paper we have presented the design and implementation of a RIS tile targeting the Wifi-6E range. The design is suited for scalability, both in terms of physical assembly as well as control. A 8x8 tile using our PIN diode based unit cell was validated in anechoic chamber environment, where we analyzed the performance for several frequencies and steering angles. Despite a deviation from the intended central frequency, we demonstrated successful steering capabilities at $6.16\,\mathrm{GHz}$, for a signal emitted by a feed horn located $40\,\mathrm{cm}$ away from the RIS. Our design will be available as open-source, accelerating research on RIS implementations and applications for WiFi-6E networks.

For future work, we are currently assembling a setup with four tiles, to evaluate the improved steering capabilities under a

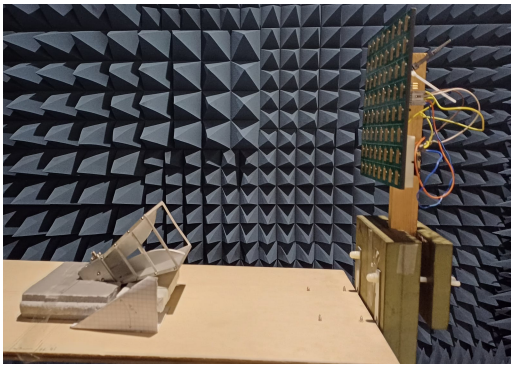

(a) relative TX to RIS positioning, with TX feed point positioned 400 mm away from center of RIS and a 35° angle

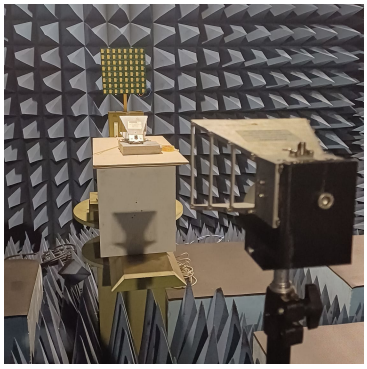

(b) RX position relative to RIS mounted on rotor

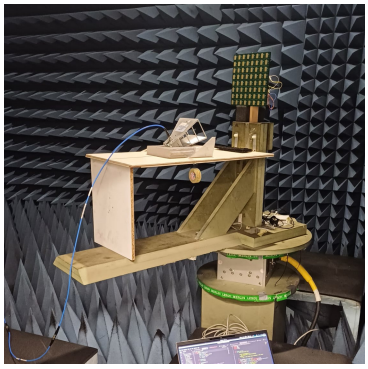

(c) rotor positioned at −60° relative to its rotation axis, with relative position between TX and RIS maintained

Fig. 6. Setup for RIS data gathering with RIS and TX mounted on a rotational platform, RX antenna on a fixed support. The VNA (not shown) and rotor control are both connected to a latop to drive automated data gathering.

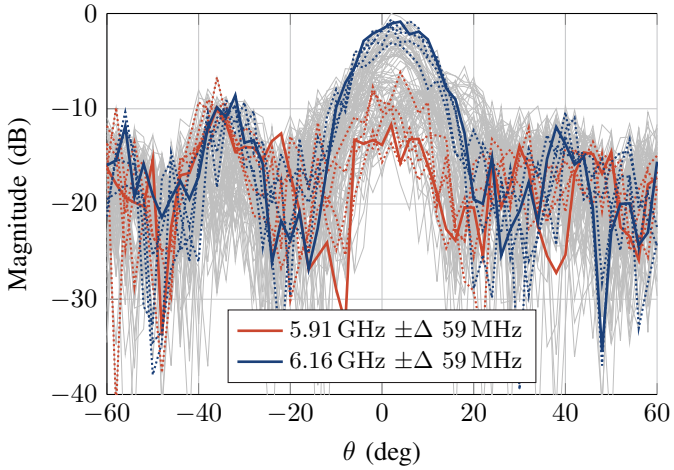

Fig. 7. RIS radiation patterns for a beamforming configuration of $\theta = 0°$ and $\phi = 0°$ (i.e, steering towards the normal vector of the RIS plane) and an angle range of $\pm 60°$, with 5.91 GHz and 6.16 GHz highlighted.

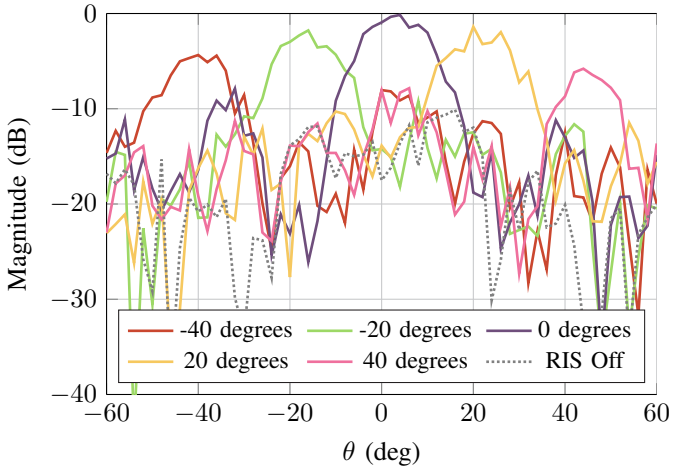

Fig. 8. RIS radiation patterns for six beamforming configurations, for 6.16 GHz, showing an effective steering capability which compensates the rotor positioning. Also shown is the specular response (i.e., RIS off).

similar setup, and will also explore the multi-beam capabilities afforded by our tile level control. Additionally, we will iterate on the unit cell design to mitigate deviations from the intended central frequency, which may include focusing on a 2-bit control, and also consider RIS designs for FR2 frequencies that retain compatibility with our controller setup.

References

[1] G. Naik, J.-M. Park, J. Ashdown, and W. Lehr, "Next generation wi-fi and 5g nr-u in the 6 ghz bands: Opportunities and challenges," *IEEE Access*, vol. 8, pp. 153 027–153 056, 2020.

[2] M. Ghoshal, S. B. Krishna, F. Gringoli, J. Widmer, and D. Koutsonikolas, "A first look at 160 mhz wifi 6/6e in action: Performance and interference characterization," in *2024 IFIP Networking Conference (IFIP Networking)*, 2024, pp. 489–495.

[3] Y. Liu, X. Liu, X. Mu, T. Hou, J. Xu, M. Di Renzo, and N. Al-Dhahir, "Reconfigurable intelligent surfaces: Principles and opportunities," *IEEE Comm. Surveys & Tutorials*, vol. 23, no. 3, pp. 1546–1577, 2021.

[4] C. Li, Q. Huang, Y. Zhou, Y. Huang, Q. Hu, H. Chen, and Q. Zhang, "Riscan: Ris-aided multi-user indoor localization using cots wi-fi," in *Proceedings of the 21st ACM Conference on Embedded Networked Sensor Systems*, 2024, p. 445–458.

[5] Y. He, D. Zhang, and Y. Chen, "High-resolution wifi imaging with reconfigurable intelligent surfaces," *IEEE Internet of Things Journal*, vol. 10, no. 2, pp. 1775–1786, 2023.

[6] A. Araghi, M. Khalily, M. Safaei, A. Bagheri, V. Singh, F. Wang, and R. Tafazolli, "Reconfigurable intelligent surface (ris) in the sub-6 ghz band: Design, implementation, and real-world demonstration," *IEEE Access*, vol. 10, pp. 2646–2655, 2022.

[7] B. G. Kashyap, P. C. Theofanopoulos, A. S. Shekhawat, A. Y. Modi, A. P. Sengar, S. K. Kumar, A. Chang, T. Osman, A. Alkhateeb, and G. C. Trichopoulos, "A reconfigurable intelligent surface for 5g wireless communication applications," in *2021 IEEE International Symposium on Antennas and Propagation and USNC-URSI Radio Science Meeting (APS/URSI)*, 2021, pp. 111–112.

[8] M. Heinrichs, A. Sezgin, and R. Kronberger, "Open source reconfigurable intelligent surface for the frequency range of 5 ghz wifi," in *IEEE Intl. Symposium On Antennas And Propagation (ISAP)*, 2023, pp. 1–2.

[9] M. Rossanese, P. Mursia, A. Garcia-Saavedra, V. Sciancalepore, A. Asadi, and X. Costa-Perez, "Open experimental measurements of sub-6ghz reconfigurable intelligent surfaces," *IEEE Internet Computing*, vol. 28, no. 2, pp. 19–28, 2024.